# Mechanical Energy Harvesting with Ferroelectrets

Xiaoqing Zhang,[1] Heinz von Seggern,[2] Gerhard M. Sessler,[3] and Mario Kupnik[4]

[1]Shanghai Key Laboratory of Special Artificial Microstructure Materials and Technology, School of Physics Science and Engineering, Tongji University, Shanghai, China; [2]Electronic Materials, Technical University of Darmstadt, Germany; [3]Institute for Telecommunications Technology, Technical University of Darmstadt, Germany; and [4]Measurement and Sensor Technology Group, Technical University of Darmstadt, Germany

**Key words:** energy harvesting, ferroelectrets, mechanical energy resource

Mechanical energy harvesting by means of ferroelectrets provides an effective way of self-powering wireless sensor networks (WSN) nodes in the rapidly developing internet of things (IoT).

## Introduction

The new internet standard 5G offers new possibilities to combine and connect different platforms like artificial intelligence (AI) and the internet of things (IoT) which will influence almost all aspects of people's lives. The connectivity of all these things will revolutionize the way information will be transferred and distributed. In 2025 the amount of connected devices will approach 75 billion worldwide, a five-time increase in the last ten years [1]. These devices can be handled in wireless sensor networks (WSN), acting in structural health monitoring, autonomous driving, smarter agriculture, etc.

Although such electronics can be powered by conventional batteries, the replacement of those can be very expensive or even impossible when many devices are operated in remote areas without power supplies or in harsh environments. A possible solution for the replacement of batteries is *Energy Harvesting*, meaning the utilization of environmental energy by converting it to electrical energy [2–5]. Fields of applications and the power required for their operation are shown in Figure 1 [6]. In principle, energy harvesting is similar to large-scale renewable energy generation of power levels of megawatts and larger, but differs in the amount of energy generated from tens of nanowatts to hundreds of milliwatts. The corresponding technology is suited for much smaller power consuming systems and, therefore, can guarantee the operation of most of the electronic devices of the IoT.

A typical energy harvesting system is composed of an energy source, the harvesting mechanism, and an electric load that utilizes the produced energy. Thereby it exploits energies from mechanical, thermal, solar, and electromagnetic radiation sources. Here we will concentrate on the conversion of mechanical to electrical energy potentially deployed in wireless sensor applications. For example, the source of mechanical energy can be a moving human body or a vibrating structure at low frequencies and reasonable accelerations (Table 1) [7], or acoustic waves at audio or ultrasonic frequencies. The transduction principles in mechanical energy harvesters are electromagnetic, piezoelectric and electrostatic. As an example, the conversion from mechanical to electrical energy in a piezoelectric energy harvester is realized by the direct piezoelectric effect. The electrical energy is then managed by an electric circuit module for various applications and for storage in rechargeable battery.

In this article, we review mechanical energy harvesting, including vibrational energy harvesting at low frequencies and acoustic energy harvesting in the audio and ultrasonic frequency ranges, utilizing piezoelectric transducers based on ferroelectret films. We discuss mostly results obtained at Technical University of Darmstadt and at Tongji University. We will, however, also mention key work done in other places, in particular, if this work has been essential for the reported results.

## Ferroelectrets

Before discussing the function of a ferroelectret-based energy harvester it is necessary to introduce the physical concept of a ferroelectret. Such a ferroelectret is the active element in a piezoelectric energy harvester. The ferroelectret is responsible for generation of electric power when applying mechanical force by the direct piezoelectric effect. The relevant physical constants are the piezoelectric $d_{33}$ coefficient (longitudinal piezoelectric effect) or $d_{31}$ coefficient (transverse piezoelectric effect) which determine principally the power efficiency of the harvester. Such a ferroelectret is a film which is made up of a combination of two different materials with strongly dissimilar elastic moduli $Y$, e.g., closed air cavities with $Y = 0.1$ MPa and a typical polymer with $Y = 300$ MPa to $Y = 2000$ MPa. Merged in the right way one obtains a very soft cellular structure, which basically relies on the softness of the air and the remain-

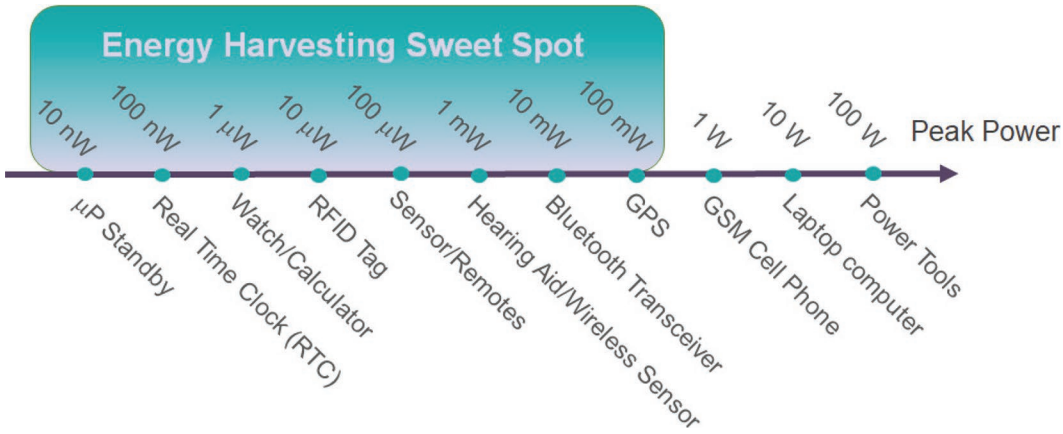


**Figure 1.** Power consumption of various electronic devices [6].

ing stiffness of the cellular structure of the involved polymer. Combining this softness with the presence of macroscopically aligned electrical dipoles across the air voids, one obtains a ferroelectret with a large piezoelectric $d_{33}$ coefficient.

## Development of Polypropylene and Fluoropolymer Ferroelectrets

Such a material in the form of cellular polypropylene (PP) was first proposed by VTT Finland [8–10], whose basic material structure is shown in Figure 2. When such a material is sandwiched between two electrodes and exposed to an electric field which exceeds the breakdown strength of air, positive and negative charge will be generated through ionization of air molecules. The resulting charges follow the electric field of the applied voltage and separate in the air cavities. If the polymer walls are able to electronically trap such charges quasi-permanently, macroscopic polarization forms with one side of the cavities charged positively and the other negatively [11]. The utilized techniques to generate such a breakdown field are numerous and range from contact poling [11–14] over corona poling [13] to radiation induced charging [15], to name just a few. The resulting piezoelectric $d_{33}$ coefficient of the VTT PP was initially between 25 to 150 pC/N [10].

Due to the inferior charge storage stability of PP [9] and its relatively high elastic modulus, research now concentrates on fluoropolymer-based hybrid structures which can be a combination of fluorinated polyethylene propylene (FEP), polytetrafluoroethylene (PTFE), expanded PTFE (ePTFE) films and closed or open porous air voids. The advantages of the fluorocarbons are their superior charge storage stability and their achievable high piezoelectric $d_{33}$ coefficients due to the small stiffness of the composite structure. An overview of some of the fluorocarbon ferroelectrets suggested in the literature is presented in Table 2. The first composite devices were FEP-electret microphones designed in the 1960s [16] which were, however, not denoted as piezoelectric systems at that time. This changed in 1999 when multilayer electrets with fluoropolymer films were suggested by Gerhard *et al*. [17] as a combination of at least one soft and one hard component. A maximum $d_{33}$ coefficient of 35 pC/N was then obtained. This line was followed in 2005 by Altafim *et al*. [18] with a $d_{33}$ coefficient of 510 pC/N and Hu *et al*. in 2006 [12] utilizing a both-sided metallized sandwich structure of 12.5 µm FEP / 63 µm ePTFE / 12.5 µm FEP bonded together by electrostatic forces. The resulting structure exhib-

**Table 1.** Accelerations and frequencies of fundamental vibration modes of various sources [7]

| Vibration Source | Acceleration ($m/s^2$) | Frequency of Peak (Hz) |
|---|---|---|
| Car engine compartment | 12 | 200 |
| Base of 3-axis machine tool | 10 | 70 |
| Blender casing | 6.4 | 121 |
| Clothes dryer | 3.5 | 121 |
| Person nervously tapping their heel | 3 | 1 |
| Car instrument panel | 3 | 13 |
| Door frame just after door closes | 3 | 125 |
| Small microwave oven | 2.5 | 121 |
| HVAC vents in office building | 0.2–1.5 | 60 |
| Windows next to a busy road | 0.7 | 100 |
| CD on notebook computer | 0.6 | 75 |
| Second story floor of busy office | 0.2 | 100 |

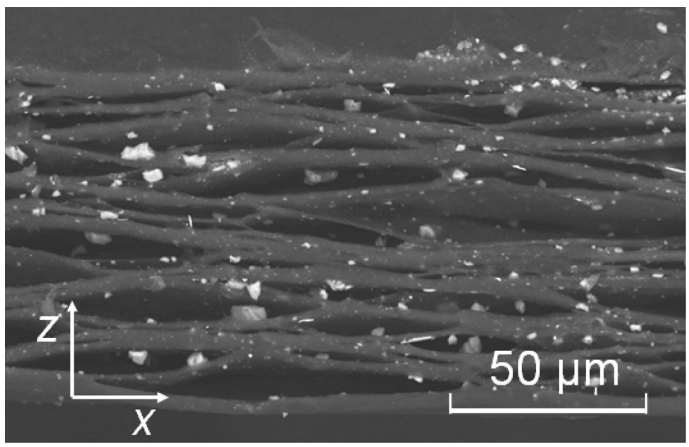


**Figure 2.** SEM image of the cross section of a cellular PP ferroelectret film.

**Table 2.** Ferroelectrets made with layered fluorocarbon films separated by air enclosures

| Description | Specific innovation | Features | References |
|---|---|---|---|
| Electret microphone | First 2-layer hard-soft system using FEP/air gap arrangement | $d_{33}$ large (not calculated at that time) | G. M. Sessler *et al.*, 1966 [16] |
| Multilayer electret system | Multi-layer hard-soft systems | $d_{33}$ = 35 pC/N | R. Gerhard *et al.*, 1999 [17] |
| Heat-bonded structure | FEP-FEP structure with pressure treated, heat-bonded (200°C) structure | $d_{33}$ = 510 pC/N | R. A. C. Altafim *et al.*, 2005 [18] |
| Electrostatically-bonded structure | Sandwich-structure FEP/ePTFE/FEP electrostatically bonded | $d_{33}$ = 800 pC/N | Z. Hu *et al.*, 2006 [14] |
| High-temperature bonded structure | High-temperature-fused (280°C) PTFE/FEP/PTFE structure | $d_{33}$ = >1000 pC/N is stable at 90°C | X. Zhang *et al.*, 2006 [20,21] |
| Tubular FEP ferroelectrets | First tubular FEP-film structure, made with PTFE template | $d_{33}$ = 160 pC/N | R. A. P. Altafim *et al.*, 2009 [23] |
| Patterned structure ferroelectrets | Rigid template to form FEP films. Fusion bonded at 290°C | After annealing, $d_{33}$ = 1000 pC/N is stable at 120°C | X. Zhang *et al.*, 2012 [22] |
| Unipolar Ferroelectrets | First use of unipolar feature in ferroelectrets (only negative charge in polymer) | $d_{33}$ ~45 pC/N (about twice as high as in PVDF) | D. Rychkov *et al.*, 2014 [24] |
| Transverse piezoelectricity in ferroelectrets | Metal template-formed and then fusion-bonded (320°C) FEP films. First ferroelectrets with large $d_{31}$ effect | $d_{31}$ = 32 pC/N (larger than for PVDF) | X. Zhang *et al.*, 2016 [27,28] |
| Tubular arrays of FEP tubes | FEP tubes deformed to stadium-like shape and then fusion bonded. Bonding areas are smaller than in older arrays | $d_{33}$ = 290 pC/N for 25 µm wall thickness | S. Zhukov *et al.*, 2018 [29,30] |

ited $d_{33}$ coefficients of up to 800 pC/N [12] and good thermal stability, the latter being obtained by a method of stabilization of the positive charge by poling at 150°C, proposed in 1984 [19]. Also, in 2006 Zhang *et al*. [20] replaced the fibrous ePTFE based air cavities by an air cell formed between two very thin PTFE layers and a 12.5 µm FEP center layer, which was used to fuse the PTFE layers together at 280°C. Shortly thereafter a quasi-static $d_{33}$ coefficient of more than 3000 pC/N was reported, which reduced to 1000 pC/N after annealing for two days at 90°C. Thereafter, the samples showed remarkable stability at this temperature considering the large $d_{33}$ coefficient [21]. Rigid metal templates were used in 2012 by Zhang *et al*. [22] who achieved thermally stable FEP ferroelectrets with regular cavity structures by utilizing a fused interface between two 12.5 µm thick FEP layers at a temperature of 290°C.

The first tubular FEP structure was published by Altafim *et al*. [23] in 2009. They fused two 50 µm thick FEP films together, partially separated by a strip-shaped PTFE template. The advantage of this fusion bonding is the fact, that FEP melts and the bond becomes very strong. After fusion at temperatures up to 300°C and cooling down to room temperature the template was removed. This process was possible due to a very weak bonding between the FEP layers and the PTFE template. After corona charging at 140°C a $d_{33}$ coefficient of 160 pC/N has been obtained. The relatively small $d_{33}$ coefficient is caused by the large thickness of the FEP layers of 50 µm.

As pointed out above, the positive charges in ferroelectrets must be stabilized to make the piezoelectric coefficients more temperature resistant [19]. This is not necessary if the ferroelectrets are designed such that only negative charges are present in the polymer films and the positive charges are located only on the electrodes, as in the electret microphone. This approach was used by Rychkov *et al*. in the so-called unipolar ferroelectrets in 2014 [24]. Later in 2018 Emmerich *et al*. [25] used a micro-system approach to reduce the size of the air gap which yielded an increased $d_{33}$ coefficient in these films. The first use of unipolar ferroelectrets in energy harvesting was carried out by Ma *et al*. in 2019 [26].

A novel approach was introduced in 2016 by Zhang *et al*. [27], utilizing 12.5 µm thick FEP films, which were deformed by a template shown in Figure. 3 (top). Thereby two FEP films were separated by a soft pad of rubber and subsequently hot pressed by the template [see Figure 3 (top)]. After removal of the soft pad the two deformed FEP films were fusion bonded by the hot template at temperatures of 320°C. This work was the first to realize a sizeable *transverse* $d_{31}$ coefficient in a ferroelectret [27]. As will be shown below, such ferroelectrets can be used to design energy harvesters with comparatively large

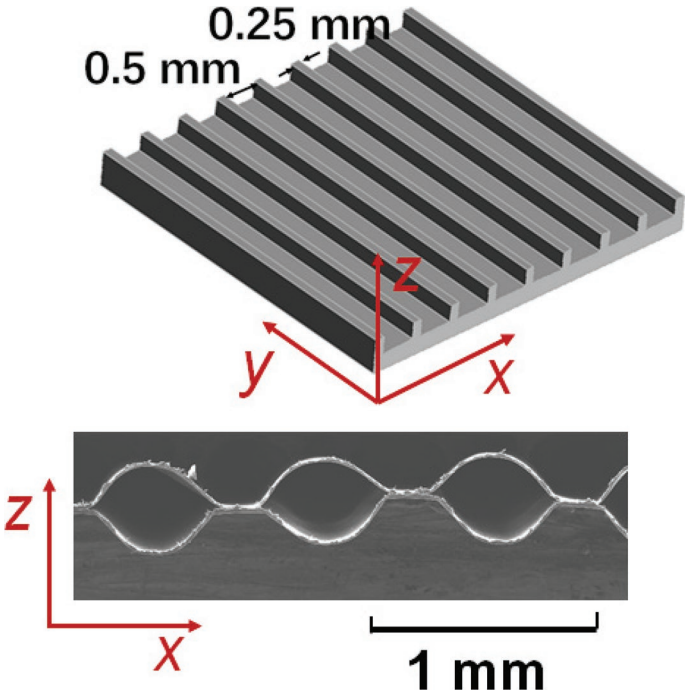


**Figure 3.** Parallel tunnel structure by Zhang et al. [27,28]: (top) Template to deform the FEP films and (bottom) resulting tunnel structure with a wall thickness of 12.5 µm, a pitch of ≈750 µm and a cavity width of 500 µm and a cavity height of 500 µm.

output power [28]. Another approach by Zhukov *et al*. [29,30] utilizes FEP tubes, which are deformed to stadium like shapes and then fusion-bonded at elevated temperatures to obtain a tube array (see Figure 4). The advantage of such structures can be seen in the larger active area compared with the parallel tunnel structure of Figure 3 (bottom). However, the disadvantage is the unavailability of tubes with very thin walls which are necessary to achieve large $d_{33}$ coefficients and therewith large output powers of energy harvester built thereof [29,30].

## Theoretical Considerations on Ferroelectrets

An early theoretical approach for an analytical description of the $d_{33}$ coefficient was based on the assumption of a simplified model having a sandwich-like structure consisting of multiple, plane-parallel solid layers separated by air gaps [9,31]. These models assume the solid layers to be incompressible and to carry charge of opposite sign on their two surfaces such that the charge layers on the two sides of each air gap are of equal magnitude and of opposite sign. The compressibility, and, thus, Young's modulus of the sandwich is assumed to originate from the morphology of the device. The $d_{33}$ coefficient obtained from this model explains to a good approximation the piezoelectric activity of the structures introduced above. In the aforementioned models the reversibility of the piezoelectric response also was shown, meaning that the material can be used to convert mechanical into electrical energy and vice versa with equal piezoelectric $d_{33}$ coefficients for the direct and reverse piezoelectric effects, as required for piezoelectric materials.

By assuming a structure, as schematically shown in Figure 4b, one obtains [29]:

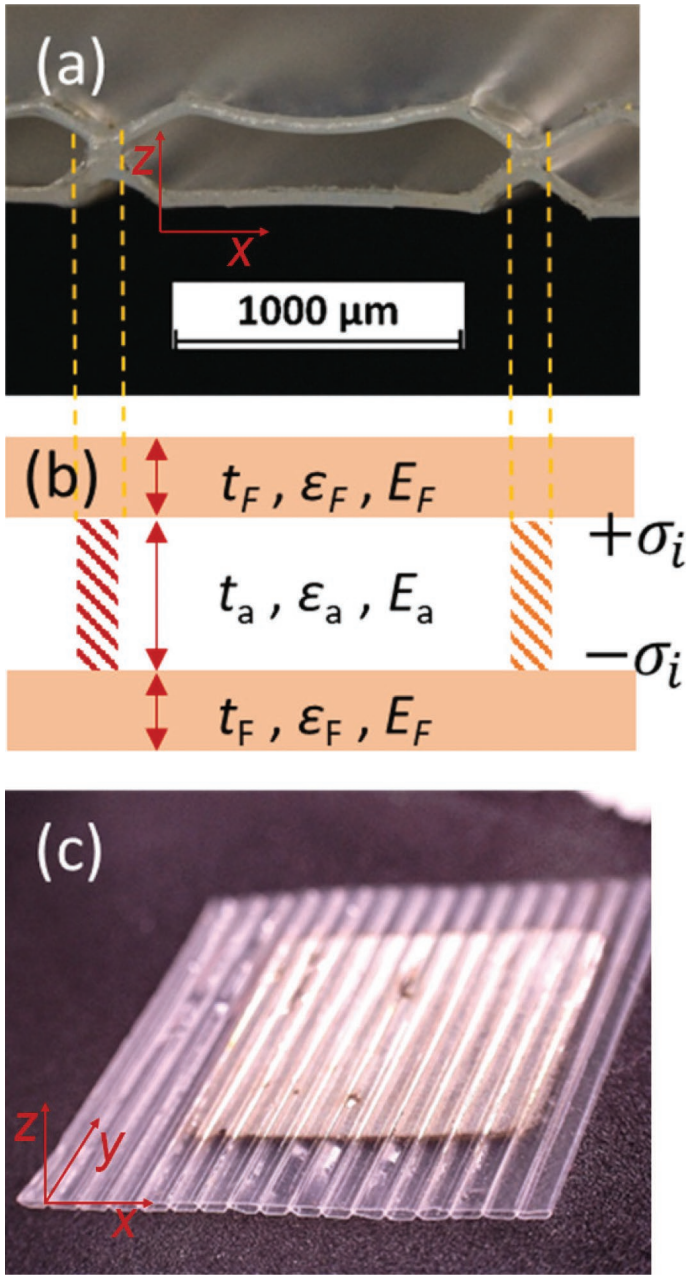


**Figure 4.** Parallel tube array by Zhukov *et al.* [29]: a) Deformed and fused FEP tubes at 270°C with a wall thickness of 50 µm, a pitch of ≈1.3 mm and an air gap of ≈250 µm, b) schematic of the ferroelectret configuration and c) photograph of the resulting tube array with Al metallization.

$$d_{33} = \frac{\Delta Q}{\Delta F} = \frac{\Delta Q / A}{\Delta F / A} = \frac{\varepsilon_0 \varepsilon_F \cdot (2t_F + t_a)}{Y} \cdot \frac{\Delta E_F}{\Delta t_a}, \quad (1)$$

where $\Delta Q$ is the generated charge by the applied force $\Delta F$, $A$ the sample area, $\varepsilon_0$, $\varepsilon_F$ and $\varepsilon_a$ the dielectric constant of vacuum, FEP and air, respectively and $\Delta F/A = \Delta\sigma_m$ the mechanical stress, which can be expressed through Hooke's law by $\Delta\sigma_m = Y \cdot \Delta t_a / (2t_F + t_a)$. $Y$ is Young's modulus of the complete structure and $t_F$ and $t_a$ the thickness of the FEP film and the air spacer, respec-

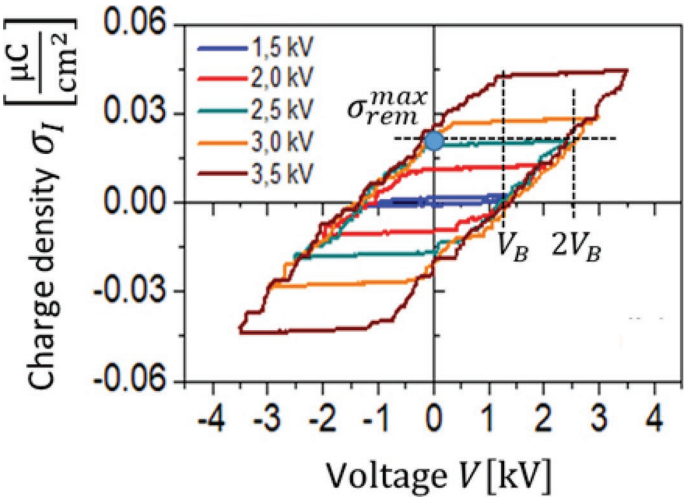


**Figure 5.** Hysteresis loop for the trapped charge density $\sigma_I$ at the interface of the solid FEP and the air gap of the tube array described in Figure 4 [29]: $\sigma_{rem}^{max}$ describes the maximal achievable trapped charge density in short circuit and $V_B$ the breakdown voltage.

tively. Utilizing Gauss's law and Kirchhoff's second law one can determine the gradient $\Delta E_F/\Delta t_a$ under short circuit conditions which amounts to

$$\frac{\Delta E_F}{\Delta t_a} = \frac{\varepsilon_0 \varepsilon_a \frac{2t_F}{t_a^2} \sigma_i}{\left(\varepsilon_0 \varepsilon_F + \varepsilon_0 \varepsilon_a \frac{2t_F}{t_a}\right)^2}. \quad (2)$$

Introducing Eq. 2 into Eq. 1, one obtains for the $d_{33}$ coefficient [29,32]:

$$d_{33} = \gamma \frac{\varepsilon_F \varepsilon_a \sigma_i}{Y} \cdot \frac{1 + t_a / 2t_F}{(\varepsilon_a + \varepsilon_F (t_a / 2t_F))^2}, \quad (3)$$

where $\pm\sigma_i$ represents the interfacial charge at the top, respectively bottom interface between the FEP layer and the cavity and $\gamma$ is a correction factor that describes the ratio between the active and the sum of active and non-active part of the device as indicated by the dashed lines in Figure 4a and the cross-hatched area in Figure 4b. Equation 3 also can be derived from Equation 3 in Ref. 31 and Equation 2 in Ref. 32 by introducing $\gamma = 1$ and $\varepsilon_a = 1$.

In addition, it is important to mention that $\sigma_i$ in the above equation is limited to a maximum value $\sigma_{rem}^{max}$ at V = 0 kV once the sample has been exposed to a voltage of at least twice the onset voltage of breakdown $V_B$. This behavior can be seen from Figure 5, where $\sigma_i$ always returns to the marked point $\sigma_{rem}^{max}$ once the applied voltage $V$ has overcome $2V_B$ and has subsequently been reduced to $V = 0$ kV. For the first cycle at $V = V_B$ $\sigma_i$ is zero and the electric field strength $E_a$ in the air cavity has reached the critical value $E_B$ for the onset of breakdown.

This leads to the generation of ionized air molecules which move to the cavity walls where they are quasi-permanently trapped. For an increasing applied voltage $V \geq V_B$ the electric field $E_a$ exceeds $E_B$, which leads to a renewed air breakdown and the thereby separated charges lead to an increase in $\sigma_i$. The increase stops when the electric field in the air gap undercuts $E_a = E_B$. This is a kind of feedback control which is valid for any arbitrary geometrical structure. $V_B$ and $E_B$ are then coupled by the geometrical and dielectric properties of the structure. For the present cavity of Figure 4 it yields [29]:

$$E_B = \left(t_a + \frac{2\varepsilon_a t_F}{\varepsilon_F}\right)^{-1} V_B. \quad (4)$$

The charge density $\sigma_i$ at $2V_B$ then becomes [29]

$$\sigma_i = \sigma_{rem}^{max} = \varepsilon_0 \left(\varepsilon_a + \varepsilon_F \frac{t_a}{2t_F}\right) E_B, \quad (5)$$

where the subscript rem stands for the remnant charge density which remains after the applied voltage has been returned to $V = 0$ kV. For applied voltages $V \geq 2V_B$ $\sigma_i$ exceeds $\sigma_{rem}^{max}$ due to the limitation of the electric field in the air gap to $E_B$. This, on the other hand, leads to a strong increase of the electric field in the cavity walls. A subsequent reduction of the applied voltage back to $V = 0$ kV initially keeps $\sigma_i = const$ until $E_a$ undercuts $-E_B$ and for smaller $V$ values breakdown-induced back-discharge starts and reduces $\sigma_i$ down to $\sigma_{rem}^{max}$ The residual hysteresis curve can be interpreted analogously.

From Equation 3 one can guess that for any geometry and dielectric material combination $d_{33}$ can be written as

$$d_{33} = (\sigma_{rem}/Y)K, \quad (6)$$

where $\sigma_{rem}$ replaces $\sigma_i$ and is limited for a given geometrical structure and material combination. $K$ is a constant which relies on the geometry and the dielectric properties of the structure. Once $\sigma_{rem}$ has reached its maximum value during poling the only parameter that can be used to increase $d_{33}$ is the reduction of Young's modulus $Y$ of the utilized device structure. Introducing $\sigma_i$ from Equation (5) into Equation (3) it yields:

$$d_{33}^{max} = \gamma \cdot \frac{\varepsilon_0 \varepsilon_F \varepsilon_a \cdot \left(1 + \frac{t_a}{2t_F}\right)}{Y \cdot \left(\varepsilon_a + \varepsilon_F \frac{t_a}{2t_F}\right)} \cdot E_B. \quad (7)$$

One realizes that this theory is applicable to structures such as shown in Figures 3b and 4b. In this case the $d_{33}$ coefficient is mainly determined by the breakdown strength of air in the air voids and by the geometrical and dielectric properties as well as Young's modulus. The Equation (7) indicates that in the present model the air gap must be as small as possible in the z-direction since the breakdown in air follows Paschen's law [33] showing

a higher breakdown field strength for smaller gaps. The remaining factor $\gamma \cdot \left(1 + \frac{t_a}{2t_F}\right) / \left(\varepsilon_a + \varepsilon_F \frac{t_a}{2t_F}\right)$ also allows to vary $d_{33}^{max}$ and assumes its maximum value for $\gamma = 1$ and $2t_F \gg t_a$ for given dielectric permittivities. A further possibility to increase $d_{33}^{max}$ is to lower Young's modulus, which at low frequencies is mainly determined by the FEP framework and not by the restoring forces of the air cushion since the utilized framework consists of open tunnels which allow for an air exchange with the surroundings. This FEP framework has to be designed in a way to be easily deformable under the desired stress from the z-direction. This design requirement limits the use of a too small air gap as just suggested to achieve a very large $E_B$. Whereas complicated frameworks have to be determined by numerical simulation [34], simple structures can be solved by a combination of models by Voigt [35] and Reuß [36] which describe Young's modulus for stress directed parallel and perpendicular to the framework elements, respectively. Another ferroelectret framework, besides the tunnel structure, is the cross-tunnel, which consists of perpendicularly arranged tunnels and will be introduced below.

Recently, the above described parallel tunnel ferroelectret has been utilized as a ferroelectric energy harvester in $d_{31}$ mode [27,28]. In these works, the parallel tunnel ferroelectret structure shown in Figure 3b can be stretched in the x direction due to a force in the z-direction and therewith the $d_{31}$ mode is activated. However, the $d_{31}$ coefficient for these samples cannot be determined directly since the required thickness of the sample in z-direction depends on the x-direction. Thus, the $g_{31}$coefficient which is independent on x has been utilized [28]. This coefficient was determined experimentally to be 3.0 Vm/N in static mode and 0.6 to 0.8 Vm/N in the dynamic mode for frequencies between 5 and 100 Hz [28]. Using this, the corresponding $d_{31}$ was calculated to be 32 pC/N. This value turned out to be much smaller than the $d_{33}$ coefficient of the same material of about 1300 pC/N. When using these films in energy harvesters in $d_{31}$ mode, the relatively small $d_{31}$ coefficient can be compensated by an appropriate design of the harvester [27,28].

## Kinetic Energy Harvesters Based on Ferroelectrets

### Kinetic Energy Harvesters Based on Ferroelectrets with Longitudinal Piezoelectric Effect, i.e., Working in 33 Mode

A brief outline of energy harvesting, including vibrational energy harvesting utilizing piezoelectric or electrostatic transduction, has been given in the Introduction. Forerunners of this technology in its electrostatic implementation were based on charged dielectrics, i.e., electrets, to generate the necessary electric field. Initially, rotating electret generators with charged or polarized wax or polymer materials were suggested [37,38]. Later, vibrational rather than rotational energy was used for conversion. In the early 2000s, a variety of miniaturized MEMS devices were introduced (see the review paper by Suzuki *et al.* about early work in this field [39,40]).

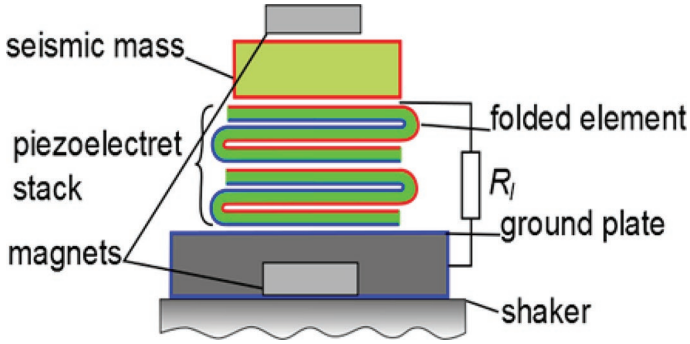


**Figure 6.** Schematic of experimental setup consisting of energy harvester and shaker. In the illustrated example, a ferroelectret stack of 6 layers, partly folded and partly stacked, is shown. The harvester is positioned on an electrodynamic shaker. This allows one to measure the electric power generated by the mechanical vibrations in the resistor $R_l$.

A ferroelectret material was first employed for energy harvesting in 2012 [41,42]. These early systems used foamed PP (Figure 2) with $d_{33}$ coefficients of only 30 pC/N and yielded relatively small power outputs of 40 nW for an acceleration of 0.5 $g$ and a seismic mass of 1 kg [42]. Later implementations with samples of larger area (230 cm$^2$) and higher $d_{33}$ coefficients (600 pC/N) delivered power outputs of up to 6 µW [41,43].

Our own work in this field also began with PP harvesters, where the PP films were arranged in stacks consisting of n films positioned between a ground plate and a seismic mass $m_s$ with the entire device placed on a shaker table (see Figure 6) [44]. This shaker excites the mass to an acceleration and thus generates the desired output power due to the longitudinal piezoelectric effect of the ferroelectret.

This design is expected to deliver a power proportional to $n^{1/2}$ and $m_s^{3/2}$ [44]. Experimentally the power output of a nine-layer system was up to 5 µW with a seismic mass of only 8 g, compared with the much larger masses in the older harvesters.

A model of such energy harvesters yields the generated power as [44]

$$P_n = P_{s,p} = \frac{m_s^2 R_l (p\, d_{33})^2 \omega^2 a_{eff}^2}{[(\frac{\omega^2}{\omega_{0,n}^2} - 1)^2 + 4\, \zeta_n^2 \frac{\omega^2}{\omega_{0,n}^2}][1 + (R_l C' \omega)^2]}. \quad (8)$$

where $m_s$ is the seismic mass, $R_l$ is the terminating resistance, p is the number of layers in a harvester consisting of a ferroelectret stack, $a_{eff}$ is the rms-value of the acceleration, $\omega_{0,n}$ is the resonance frequency of the harvester, and $\zeta_n$ is the damping ratio. The normalized power $P_n$ is defined as

$$P_n = P\,(g/a)^2, \quad (9)$$

As one notes from Equation (8), the power output of such harvesters rises with $\omega^2$ below the resonance frequency and

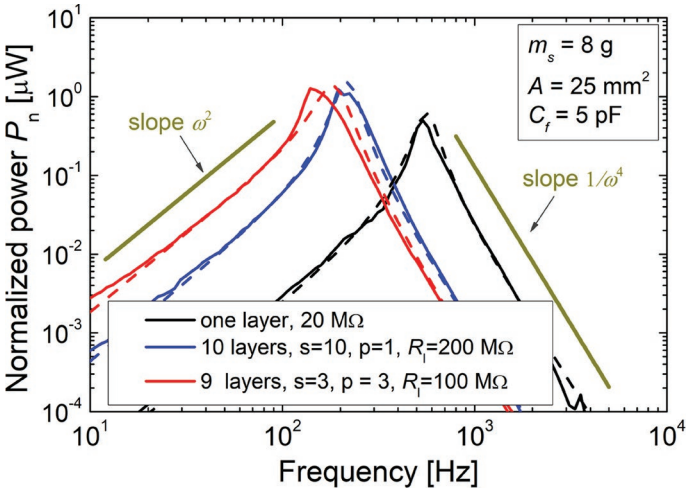


**Figure 7.** Power generated by energy harvesters with various numbers of ferroelectret layers. Full lines represent measurements, dashed lines are simulation results. The resonance frequency generally decreases with increasing number of layers because of the increased mass loading.

falls with $1/\omega^4$ well above resonance (Figure 7). The increase of the generated power with $n^{1/2}$ is seen in the plots. (with a deviation when going from 9 to 10 layers, due to slight non-reproducibilities of the layers). Other features of energy harvesters, such as the just mentioned dependence of the power on seismic mass or on acceleration $a$ (proportional to $a^2$), were also confirmed. Later experiments with radiation-crosslinked PP (IXPP), that shows better thermal stability and somewhat improved piezoelectric performance [45], resulted in an output power in excess of 100 μW.

All PP ferroelectrets show a sizeable longitudinal $d_{33}$ piezoeffect but very small transverse $d_{31}$ activity. Another drawback of the PP is the poor thermal electret stability which is responsible for a decay of the piezoelectric coefficients, and thus of the harvester output, above 50°C. Ferroelectrets that are thermally much more stable are the above-described FEP parallel-tunnel or parallel tubes samples (Figures 3 and 4) or, as a modification of these, the cross-tunnel samples [46]. The latter were the first FEP ferroelectrets used for energy harvesting, still utilizing the piezoelectric thickness mode ($d_{33}$) [46]. As expected, $P_n$ as a function of the terminating resistance $R_l$ showed a peak at a resistance that obeys the relation $R_l = 1/\omega_0 C$, where $C$ is the capacitance of the ferroelectret including parasitic capacitances and $\omega_0$ is the resonance frequency. The findings for the FEP parallel-tunnel harvesters with respect to frequency response, resonance frequency, seismic mass, and other parameters are similar for the PP and the FEP harvesters.

## Kinetic Energy Harvesters Based on Ferroelectrets with a Transverse Piezoelectric Effect, i.e., Working in 31 Mode

As discussed above, the PP ferroelectrets show only a very small transverse piezoelectric effect $d_{31}$. This is very different for the FEP parallel-tunnel films. The physical reason for this difference is the much smaller Young's modulus $Y_1$ in the x-direction (Figure 3 (bottom)) of the FEP films, compared with the cellular PP material, with typical values of 1 MPa and ~100 MPa, respectively [13,28]. The large compliance of the FEP films in the x-direction will increase the Poisson's ratio and thus enhance $d_{31}$ and $g_{31}$, where $d_{31} = g_{31}\varepsilon_0\varepsilon_r$, with values of $g_{31}$ = 3.0 Vm/N for parallel-tunnel ferroelectrets [28].

The large transverse piezoelectricity has been used to design an energy harvester with increased power output (Figure 8a) [27,28]. The ferroelectret film is fixed on both sides on the support and carries a small seismic mass, cemented onto its center that exerts a force on the film when accelerated by

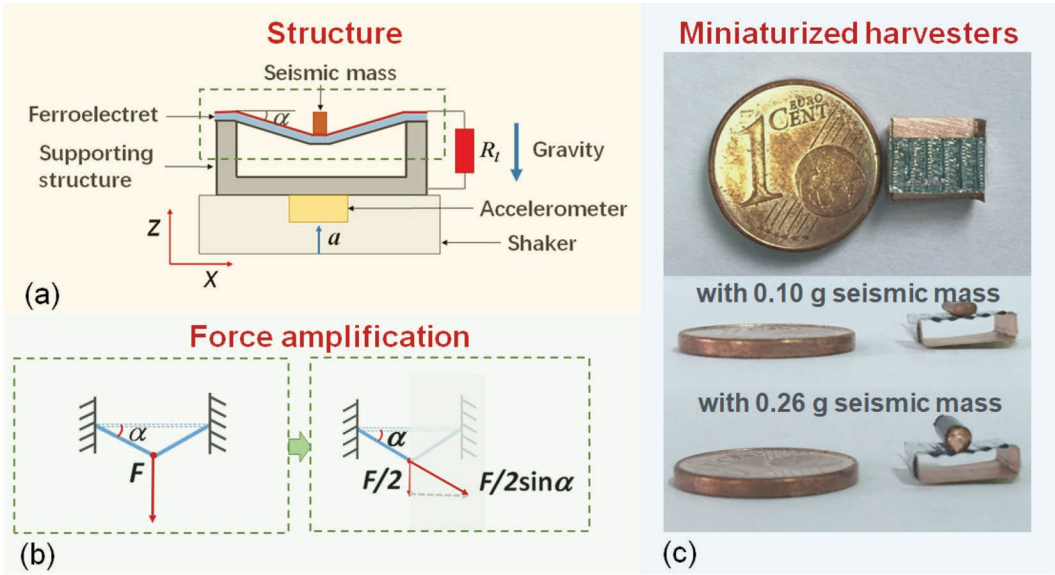


**Figure 8.** (a) Schematic of energy harvester utilizing the transverse piezoelectric $d_{31}$ activity [28], (b) primary force $F$ acting on the ferroelectret (left) and enlarged force component $F$/sin$\alpha$ within the left part of the ferroelectret and (c) miniaturized harvesters with different seismic masses.

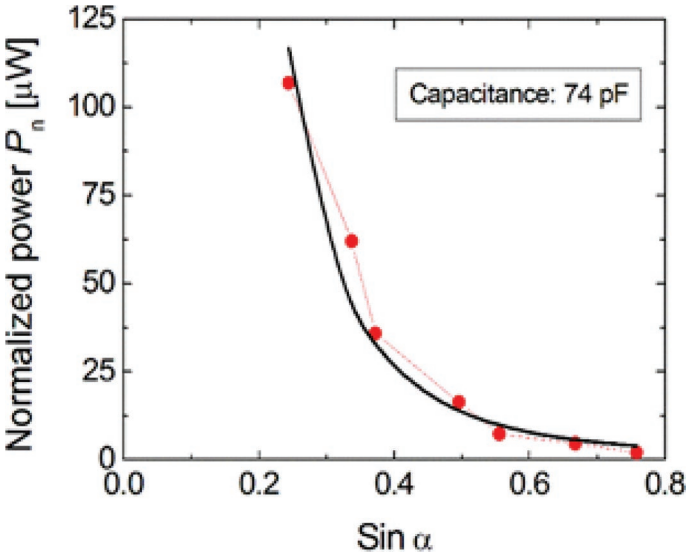


**Figure 9.** Dependence of normalized power on sin α of the harvester shown in Figure 8a. Symbols are experimental points, the line is a best fit of the function $(\sin \alpha)^{-3}$ to the experimental data [27].

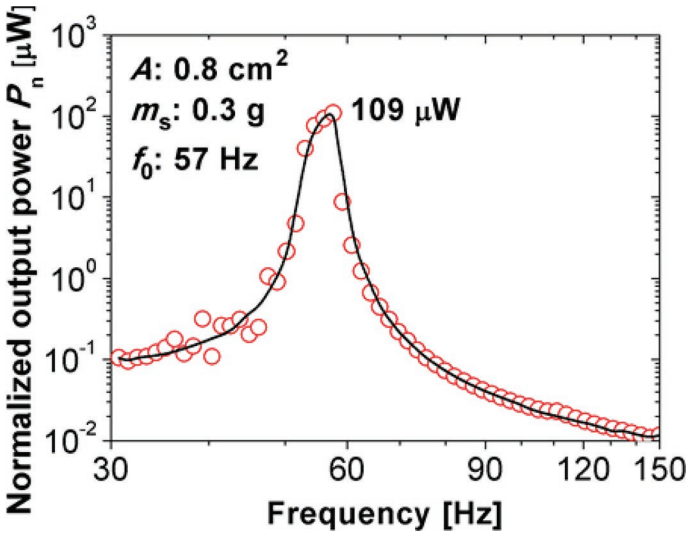


**Figure 10.** Measured normalized power of the harvester shown in Figure 8a [28].

the shaker. The stress is in the length direction (x-direction in figure 3) of the ferroelectret and results in a periodic stretching causing a corresponding thickness variation of the tunnels and thus a piezoelectric output current between the electrodes on the surfaces of the film. This generates a power in the terminating resistor $R_L$. Miniature implementations of this harvester have dimensions of only 3 × 5 × 8 mm³ (Figure 8c) [28].

The harvester in Figure 8a utilizes a kind of force amplification that results in a force *within the ferroelectret* (in the direction of its length) that significantly exceeds the force generated by the acceleration of the seismic mass *in the vertical direction*. This is seen from Figure 8b, which illustrates the primary force $F$ exerted in vertical direction by the seismic mass on the ferroelectret (Figure 8b, left) and the enhanced force component $F/2\sin\alpha$ on the left part of the ferroelectret (Figure 8b, right).

While Figure 8b shows the enhancement of the force due to the design of the harvester, the power increases even more, namely proportional to $1/(\sin \alpha)^2$ with decreasing α [27]. The output power measured as function of the angle α is compared with the theoretical results for an energy harvester with a seismic mass of 2 g. The measured data displayed in Figure 9 confirm the simulations in the range $0.24 < \sin \alpha < 0.76$ which correspond to $14° < \alpha < 50°$. For smaller angles, the stretching forces in the ferroelectret become larger and the experiment, as well as the theory, fails. For a smaller angle, the stretching ratio of the ferroelectret becomes large which deforms the tubes to a flat, lens-like geometry and thus invalidates the theory.

The frequency dependence of the output power indicates the resonance of the system to be at about 55 Hz (Figure 10). This is in the desired frequency range for energy harvesting below 100 Hz where most of the natural or man-made vibrations occur. For a seismic mass of 0.3 g, the relatively large normalized power of more than 100 μW is generated.

## Acoustic Energy Harvesters Based on Ferroelectrets

Apart from the low-frequency vibration energy, acoustic energy is an abundant and clean mechanical energy source in both domestic and industrial environments and, therefore, has a great potential for energy harvesting [47,48]. Acoustic energy harvesting is not only an approach to obtain renewable energy for WSN, but also a promising strategy for noise reduction. There are two key issues involved in acoustic energy harvesting. One is the amplification of sound pressure, and the other is the transduction mechanism. Since acoustic energy has low energy density, various approaches to collect the ambient sound waves and to amplify the sound pressure have been investigated. Devices such as Helmholtz, quarter-wavelength, and half-wavelength resonators, acoustic metamaterials, phononic crystals, and broadband gradient-index lenses are adopted to amplify the incident sound pressure. With respect to the transduction mechanism, piezoelectric, electromagnetic, triboelectric principles are commonly utilized to convert acoustic energy into electrical energy. Compared with conventional piezoelectric materials, such as lead zirconate titanate (PZT) and polyvinylidene fluoride (PVDF) which are normally used as transduction materials in acoustic energy harvesting, ferroelectrets are more appropriate for acoustic energy harvesting in air media due to their very small acoustic impedance (~0.03 MRayl), high figure of merit ($\text{FoM} = d_{33} \cdot g_{33}$, ~11GPa$^{-1}$), flat response in audio and low-frequency ultrasonic ranges (<400 kHz), flexibility, and environmental friendliness.

Xue *et al*. adopted a Helmholtz resonator to amplify the sound pressure and utilized IXPP ferroelectret films as transduction material to harvest audible sound energy where the IXPP films work at non-resonance frequencies [49]. In their work, they also explored ultrasonic energy harvesting with the same material without a Helmholtz resonator. However, this

device worked at resonance. When the frequency $\omega$ of the incident sound is much smaller than the resonance of the ferroelectret film sample $\omega_f$ ($\omega \ll \omega_f$), and a terminal load resistance $R_l = 1/\omega C$ is selected, the optimal output $P_{out}$ of the ferroelectret acoustic harvester is given by [49]

$$P_{opt} = 0.5td_{33}g_{33}p^2A\omega, \tag{10}$$

where $p$ is the sound pressure, $A$ the area of the film sample, and $t$ the thickness of the ferroelectret film sample. The maximum output power can be obtained at the resonance frequency and amounts to

$$P_m = \frac{p^2Ad_{33}g_{33}\omega_f^2 t}{8\zeta_m^2}, \tag{11}$$

where $\zeta_m$ is the damping ratio. These two equations clearly indicate that IXPP ferroelectret films with a large FoM of 19 GPa$^{-1}$ in [49] are ideal transduction materials for acoustic energy harvesting.

In the above mentioned work by Xue *et al*. [49] an acoustic energy harvester using a Helmholtz resonator with a designed resonance frequency of 900 Hz was realized. An output power of 10.3 nW was achieved by a 16 cm$^2$ large IXPP film attached to one of the inner walls of the Helmholtz resonator, with an optimized load resistance of 962 kΩ under an incident Sound Pressure Level (SPL) of 100 dB (Figure 11a). For the same incident sound wave, the output power of the device was further improved to 43 nW by increasing the active area of the ferroelectret film, where five inner walls were covered with IXPP ferroelectrets (Figure 11b).

Relevant results on ultrasonic energy harvesting without acoustic amplification by a Helmholtz resonator reported in [49] show that a maximum output power of 7.2 nW was obtained utilizing a 16 cm$^2$ large IXPP ferroelectret film harvester at resonance frequency of 53 kHz and an incident sound pressure of 100 dB. Compared with acoustic energy harvesters us-

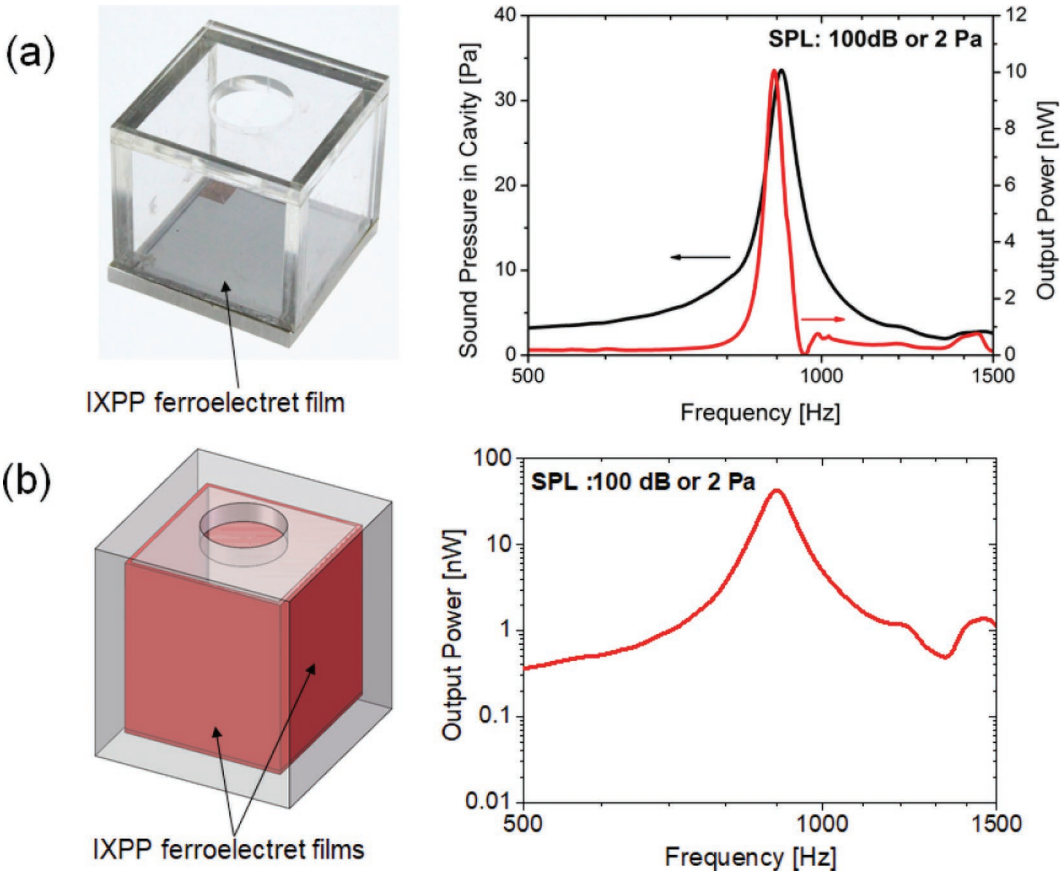


**Figure 11.** (a) Photograph of an acoustic energy harvester with an IXPP ferroelectret film attached to the bottom wall of the Helmholtz resonator (left), and measured sound pressure in the cavity and output power of the low-frequency IXPP acoustic energy harvester acquired from the short-circuit charge obtained at an input SPL of 100 dB (right). The IXPP film used has a square shape with an active area of 16 cm$^2$ and quasi-static $d_{33}$ coefficient of 550 pC/N. The device has a capacitance of 185 pF and an optimal load resistance of 962 kΩ. (b) Schematic view (left) and generated output power of an acoustic energy harvester consisting of a Helmholtz resonator with five inner walls attached with IXPP films at an input SPL of 100 dB. The IXPP films have a square shape with total active area of 80 cm$^2$ and quasi-static $d_{33}$ coefficient of 550 pC/N. The optimal load resistance of the device is 280 kΩ [49].

ing PVDF cantilever beams working in 31 mode at a specific resonant frequency, the IXPP ferroelectret acoustic energy harvesters produce a higher power density under the same conditions, yet featuring a much simpler structure because ferroelectret films work in 33 mode and at broad non-resonance frequencies. In addition, ferroelectret films also have good performance when they work at resonant frequency compared with PVDF cantilever beams.

## Conclusions and Perspectives

Vibrational or acoustic energy harvesting with ferroelectrets is a relatively new field, dating back only to 2012. We have started our work in this field in 2014 with experiments exploiting the longitudinal piezoelectric effect by employing energy harvesters utilizing the $d_{33}$ activity. The initial material used was cellular PP which was soon replaced by the thermally more stable FEP in the form of layered cellular films. The first use of the transverse piezoelectric effect was with such layered ferroelectrets. They had $g_{31}$ coefficients of up to 0.8 Vm/N, several times larger than the value for PVDF. With such harvesters a normalized power of 50 to 100 μW was achieved for seismic masses in the range of 0.1 to 0.3 g. The large effect was possible because of a force enlargement obtained from the harvester design.

These results should be compared with data available in the literature for the more classical energy harvesters operating with ceramic piezoelectric materials, such as PZT or with the polymer PVDF. Such a comparison is possible by using Figures of Merit (FoM's) that have been proposed in the literature. One such FoM is the "Normalized Volumetric Power Density" $P_N$ that has recently been evaluated for several ceramic harvesters [50]. This FoM is defined as

$$P_N = (2\pi P)/(v\omega_0 a^2), \quad (12)$$

where $P$ is the harvested power in μW, $v$ the volume of the ferroelectric material in mm$^3$, $\omega_0$ is the resonance frequency in Hz, and $a$ the acceleration in terms of $g$. The authors of [50] have applied this to 14 small-scale harvesters with PZT or aluminum nitride (AlN) as electroactive material. These harvesters have $P_N$-values between 0.19 and 9 × 10$^{-5}$ while our harvester has a value of 0.12 and is therefore close to the top-performing ceramic system.

Apart from this, there are other advantages of the present ferroelectret harvesters. These are low cost, mechanical flexibility, environmental suitability, and better matching of the mechanical impedance in many applications. Taking into consideration that the harvesters described in this paper have only been around for few years, while the conventional ceramic systems have been introduced more than 20 years ago, the present approach is very promising.

## Acknowledgments

Financial support from the Natural Science Foundation of China (NSFC, 61761136004) and the Deutsche Forschungsgemeinschaft (DFG, German Research foundation, KU 3498/1-1, SE 941/19-1, SE 941/21-1) is gratefully acknowledged.

## References

[1] http://www.statista.com/, 2019.
[2] J. A. Paradiso and T. Starner, "Energy scavenging for mobile and wireless electronics," *IEEE Pervasive Comput.*, vol. 4, no. 1, pp. 18–27. https://doi.org/10.1109/MPRV.2005.9 2005.
[3] P. D. Mitcheson, E. M. Yeatman, G. K. Rao, A. S. Holmes, and T. C. Green, "Energy harvesting from human and machine motion for wireless electronic devices," *Proc. IEEE*, vol. 96, no. 9, pp. 1457–1486. https://doi.org/10.1109/JPROC.2008.927494 2008.
[4] N. Elvin and A. Erturk, *Advances in energy harvesting methods*. Springer Science & Business Media, 2013.
[5] P. Basset, E. Blokhina, and D. Galayko, *Electrostatic Kinetic Energy Harvesting*. ISTE Ltd. and John Wiley & Sons. 2016.
[6] https://www.psma.com/HTML/newsletter/Q2_2012/page8.html.
[7] S. Roundy, P. K. Wright, and J. Rabaey, "A Study of Low Level Vibrations as a Power Source for Wireless Sensor Nodes," *Comput. Commun.*, vol. 26, no. 11, pp. 1131–1144. https://doi.org/10.1016/S0140-3664(02)00248-7 2003.
[8] A. Savolainen and K. Kirjavainen, "Electrothermomechanical Film. Part I. Design and Characteristics," *Journal of Macromolecular Science: Part A - Chemistry*, vol. 26, no. 2–3, pp. 583–591. https://doi.org/10.1080/00222338908051994 1989.
[9] M. Paajanen, H. Välimäki, and J. Lekkala, "Modelling the electromechanical film (EMFi)," *J. Electrost.*, vol. 48, no. 3, pp. 193–204. https://doi.org/10.1016/S0304-3886(99)00065-0 2000.
[10] J. Lekkala, R. Poramo, K. Nyholm, and K. Kaikkonen, "EMF force sensor-a flexible and sensitive electret film for physiological applications," *Medical& Biological Engineering & Computing,* vol. 34, no. Supplement 1, p. 67–68, 1996.
[11] S. Bauer, R. Gerhard-Multhaupt, and G. M. Sessler, "Ferroelectrets: soft electroactive foams for transducers," *Phys. Today*, vol. 57, no. 2, pp. 37–43. https://doi.org/10.1063/1.1688068 2004.
[12] Z. Sun, X. Zhang, Z. Xia, X. Qiu, W. Wirges, R. Gerhard, C. Zeng, C. Zhang, and B. Wang, "Polarization and piezoelectricity in polymer films with artificial void structure," *Appl. Phys., A Mater. Sci. Process.*, vol. 105, no. 1, pp. 197–205. https://doi.org/10.1007/s00339-011-6481-2 2011.
[13] G. S. Neugschwandtner, R. Schwödiauer, M. Vieytes, S. Bauer-Gogonea, S. Bauer, J. Hillenbrand, R. Kressmann, G. M. Sessler, M. Paajanen, and J. Lekkala, "Large and broadband piezoelectricity in smart polymer-foam space-charge electrets," *Appl. Phys. Lett.*, vol. 77, no. 23, pp. 3827–3829. https://doi.org/10.1063/1.1331348 2000.
[14] Z. Hu and H. von Seggern, "Breakdown-induced polarization buildup in porous fluoropolymer sandwiches: a thermally stable piezoelectret," *J. Appl. Phys.*, vol. 99, no. 2, p. 024102. https://doi.org/10.1063/1.2161825 2006.
[15] Y. Feng, K. Hagiwara, Y. Iguchi, and Y. Suzuki, "Trench-filled cellular parylene electret for piezoelectric transducer," *Appl. Phys. Lett.*, vol. 100, no. 26, p. 262901. https://doi.org/10.1063/1.4730952 2012.
[16] G. M. Sessler and J. E. West, "Foil-electret microphones," *J. Acoust. Soc. Am.*, vol. 40, no. 6, pp. 1433–1440. https://doi.org/10.1121/1.1910245 1966.
[17] R. Gerhard-Multhaupt, Z. Xia, W. Kunstler, and A. Pucher, "Preliminary study of multi-layer space-charge electrets with piezoelectric properties from porous and non-porous Teflon

films," in *10th International Symposium on Electrets (ISE 10). Proceedings (Cat. No.99 CH36256)*, 1999.

[18] R. A. C. Altafim, H. Basso, L. G. Neto, L. Lima, R. A. P. Altafim, and C. de Aquino, "Piezoelectricity in multi-air voids electrets," in *Electrical Insulation and Dielectric Phenomena, 2005. CEIDP'05. 2005 Annual Report Conference on*, 2005, pp. 669–672: IEEE.

[19] H. von Seggern and J. E. West, "Stabilization of positive charge in fluorinated ethylene propylene copolymer," *J. Appl. Phys.*, vol. 55, no. 7, pp. 2754–2757. https://doi.org/10.1063/1.333281 1984.

[20] X. Zhang, J. Hillenbrand, and G. M. Sessler, "Thermally stable fluorocarbon ferroelectrets with high piezoelectric coefficient," *Appl. Phys., A Mater. Sci. Process.*, vol. 84, no. 1–2, pp. 139–142. https://doi.org/10.1007/s00339-006-3573-5 2006.

[21] X. Zhang, J. Hillenbrand, and G. M. Sessler, "Ferroelectrets with improved thermal stability made from fused fluorocarbon layers," *J. Appl. Phys.*, vol. 101, no. 5, p. 054114. https://doi.org/10.1063/1.2562413 2007.

[22] X. Zhang, J. Hillenbrand, G. M. Sessler, S. Haberzettl, and K. Lou, "Fluoroethylenepropylene ferroelectrets with patterned microstructure and high, thermally stable piezoelectricity," *Appl. Phys., A Mater. Sci. Process.*, vol. 107, no. 3, pp. 621–629. https://doi.org/10.1007/s00339-012-6840-7 2012.

[23] R. A. P. Altafim, X. Qiu, W. Wirges, R. Gerhard, R. A. C. Altafim, H. C. Basso, W. Jenninger, and J. Wagner, "Template-based fluoroethylenepropylene piezoelectrets with tubular channels for transducer applications," *J. Appl. Phys.*, vol. 106, no. 1, p. 014106. https://doi.org/10.1063/1.3159039 2009.

[24] D. Rychkov, R. A. P. Altafim, and R. Gerhard, "Unipolar ferroelectrets – following the example of the electret microphone more closely," 2014 *Annual Report Conference on Electrical Insulation and Dielectric Phenomena*, pp. 860 – 862.

[25] F. Emmerich and C. Thielemann, "Optimizing dimensions of unipolar Teflon-FEP piezoelectrets with micro-system-technology," *J. Phys. Conf. Ser.*, vol. 1052, p. 012052. https://doi.org/10.1088/1742-6596/1052/1/012052 2018.

[26] X. Ma, X. Zhang, G. M. Sessler, L. Chen, X. Yang, Y. Dai, and P. He, "Energy harvesters based on fluorinated ethylene propylene unipolar ferroelectrets with negative charges," *AIP Adv.*, vol. 9, no. 12, p. 125334. https://doi.org/10.1063/1.5086113 2019.

[27] X. Zhang, P. Pondrom, L. Wu, and G. M. Sessler, "Vibration-based energy harvesting with piezoelectrets having high $d_{31}$ activity," *Appl. Phys. Lett.*, vol. 108, no. 19, p. 193903. https://doi.org/10.1063/1.4948649 2016.

[28] X. Zhang, P. Pondrom, G. M. Sessler, and X. Ma, "Ferroelectret nanogenerator with large transverse piezoelectric activity," *Nano Energy*, vol. 50, pp. 52–61. https://doi.org/10.1016/j.nanoen.2018.05.016 2018.

[29] S. Zhukov, D. Edergoy, S. Fedosov, B. X. Xu, and H. von Seggern, "Analytical prediction of the piezoelectric $d_{33}$," *Sci. Rep.*, vol. 8, no. 1, p. 4597. https://doi.org/10.1038/s41598-018-22918-1 2018.

[30] S. Zhukov, H. von Seggern, X. Zhang, Y. Xue, O. Ben Dali, P. Pondrom, G. M. Sessler, and M. Kupnik, "Microenergy harvesters based on fluorinated ethylene propylene piezo-tubes," *Adv. Eng. Mater.*, vol. 22, no. 5, p. 1901399. https://doi.org/10.1002/adem.201901399 2020.

[31] G. Sessler and J. Hillenbrand, "Electromechanical response of cellular electret films," *Appl. Phys. Lett.*, vol. 75, no. 21, pp. 3405–3407. https://doi.org/10.1063/1.125308 1999.

[32] X. Zhang, J. Hillenbrand, and G. M. Sessler, "Improvement of piezoelectric activity of cellular polymers using a double-expansion process," *J. Phys. D Appl. Phys.*, vol. 37, no. 15, pp. 2146–2150. https://doi.org/10.1088/0022-3727/37/15/015 2004.

[33] F. Paschen, "Über die zum Funkenübergang in Luft, Wasserstoff und Kohlensäure bei verschiedenen Drucken erforderliche Potentialdifferenz," *Ann. Phys.*, vol. 273, no. 5, pp. 69–96. https://doi.org/10.1002/andp.18892730505 1889.

[34] E. Tuncer, "Structure–property relationship in dielectric mixtures: application of the spectral density theory," *J. Phys. D Appl. Phys.*, vol. 38, no. 2, pp. 223–234. https://doi.org/10.1088/0022-3727/38/2/006 2005.

[35] W. Voigt, "Über die Beziehung zwischen den beiden Elasticitätsconstanten isotroper Körper," *Ann. Phys.*, vol. 274, no. 12, pp. 573–587. https://doi.org/10.1002/andp.18892741206 1889.

[36] A. Reuss, ""Berechnung der Fließgrenze von Mischkristallen auf Grund der Plastizitätsbedingung für Einkristalle," *ZAMM - Journal of Applied Mathematics and Mechanics*," *Z. Angew. Math. Mech.*, vol. 9, no. 1, pp. 49–58. https://doi.org/10.1002/zamm.19290090104 1929.

[37] Tada and Yasufusa "Experimental characteristics of electret generator, using polymer film electrets," *Jpn. J. Appl. Phys.*, vol. 31, no. 3, pp. 846–851, 1992.

[38] O. D. Jefimenko and D. K. Walker, "Electrostatic current generator having a disk electret as an active element," *IEEE Trans. Ind. Appl.*, vol. IA-14, no. 6, pp. 537–540. https://doi.org/10.1109/TIA.1978.4503588 1978.

[39] Y. Suzuki, "Electret based vibration energy harvester for sensor network," in *Solid-State Sensors, Actuators and Microsystems (TRANSDUCERS), 2015 Transducers-2015 18th International Conference on*, 2015, pp. 43–46: IEEE.

[40] Y. Suzuki, "Recent progress in MEMS electret generator for energy harvesting," *IEEJ Trans. Electr. Electron. Eng.*, vol. 6, no. 2, pp. 101–111. https://doi.org/10.1002/tee.20631 2011.

[41] S. R. Anton and K. M. Farinholt, "Piezoelectret foam-based vibration energy harvester for low-power energy generation," in *ASME 2012 Conference on Smart Materials, Adaptive Structures and Intelligent Systems*, 2012, pp. 929–937: American Society of Mechanical Engineers.

[42] S. R. Anton and K. M. Farinholt, "An evaluation on low-level vibration energy harvesting using piezoelectret foam," *Active and Passive Smart Structures and Integrated Systems 2012, edited by Henry A. Sodano, Proc. of SPIE*, vol. 8341, p. 83410G, 2012.

[43] S. R. Anton, K. M. Farinholt, and A. Erturk, "Piezoelectret foam–based vibration energy harvesting," *J. Intell. Mater. Syst. Struct.*, vol. 25, no. 14, pp. 1681–1692. https://doi.org/10.1177/1045389X14541501 2014.

[44] P. Pondrom, J. Hillenbrand, G. M. Sessler, J. Bös, and T. Melz, "Vibration-based energy harvesting with stacked piezoelectrets," *Appl. Phys. Lett.*, vol. 104, no. 17, p. 172901. https://doi.org/10.1063/1.4874305 2014.

[45] X. Zhang, L. Wu, and G. M. Sessler, "Energy harvesting from vibration with cross-linked polypropylene piezoelectrets," *AIP Adv.*, vol. 5, no. 7, p. 077185. https://doi.org/10.1063/1.4928039 2015.

[46] X. Zhang, G. M. Sessler, and Y. Wang, "Fluoroethylenepropylene ferroelectret films with cross-tunnel structure for piezoelectric transducers and micro energy harvesters," *J. Appl. Phys.*, vol. 116, no. 7, p. 074109. https://doi.org/10.1063/1.4893367 2014.

[47] M. Yuan, Z. Cao, J. Luo, and X. Chou, "Recent developments of acoustic energy harvesting: a review," *Micromachines (Basel)*, vol. 10, no. 1, p. 48. https://doi.org/10.3390/mi10010048 2019.

[48] J. Choi, I. Jung, and C. Y. Kang, "A brief review of sound energy harvesting," *Nano Energy*, vol. 56, pp. 169–183. https://doi.org/10.1016/j.nanoen.2018.11.036 2019.
[49] Y. Xue, J. Zhao, X. Zhang, G. M. Sessler, and M. Kupnik, "Acoustic energy harvesting with irradiated cross-linked polypropylene piezoelectret films," *Phys. Scr.*, vol. 94, no. 9, p. 095002. https://doi.org/10.1088/1402-4896/ab00bd 2019.
[50] S. Priya, H.-C. Song, Y. Zhou, R. Varghese, A. Chopra, S.-G. Kim, I. Kanno, L. Wu, D. S. Ha, J. Ryu, and R. G. Polcawich, "A review on piezoelectric energy harvesting: materials, methods, and circuits," *Energy Harvesting and Systems*, vol. 4, no. 1, pp. 3–39. https://doi.org/10.1515/ehs-2016-0028 2017.

**Xiaoqing Zhang** received her PhD degree in Condensed Matter Physics from Tongji University, China in 2001. From April 2001 to December 2004, she was a postdoctoral fellow, working on the dielectric properties of the inorganic dielectric materials and the piezoelectric properties of the polymer films, at Darmstadt University of Technology, Germany. She has been a full professor and the leader of the research group of Electrets and Functional Dielectrics at Tongji University since December 2010. Her interests are electro-active materials and their applications. She has over 100 scientific publications and holds 16 patents. She is a co-editor of the European Journal of Electrical Engineering (EJEE), a member of the academic committees of the IEEE International Conference on Electrets, the International Conference on Vibration and Energy Harvesting Applications, and Chinese National Conference on Electrets. She is a senior IEEE member.

**Heinz von Seggern** studied physics at the University of Goettingen and Hannover in the field of solid state physics where he graduated in 1976. He received his PhD degree from the Technical University of Darmstadt in 1979, then became Postdoc and later principal investigator at AT&T Bell Laboratories, Murray Hill, New Jersey, USA. In 1982 his work was honoured by the Physics Prize of the Academy of Science of Goettingen. In 1985 he accepted a position as principal investigator at Siemens Research Center in Erlangen where he was promoted in 1990 to department head. In 1997 he was appointed to full professor at the Technical University of Darmstadt. His scientific interests are directed toward electrical properties of dielectrics, organic electronics (OFET, OLED) and towards medical imaging. He has published over 280 scientific papers in peer-reviewed journals.

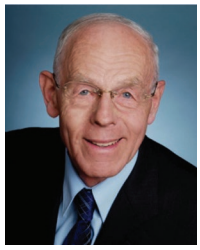

**Gerhard M. Sessler** is a graduate of the University of Goettingen in Germany. He joined Bell Laboratories in Murray Hill, N.J. and was co-inventor of the first polymer electret microphone which became the predominant microphone type. In 1975, he was appointed a professor at the Technical University Darmstadt, Germany and was involved in MEMS technology. In 1983, he and his coworkers designed the first MEMS condenser microphones which are now the leading microphone types worldwide. He is an inductee of the National Inventors Hall of Fame and recipient of the jointly granted James Clark Maxwell Award by the IEEE and the Scottish Royal Academy of Science. Presently, he is an Emeritus Professor and he and his group are working on the new ferroelectret materials and their applications.

**Mario Kupnik** received Diplom-Ingenieur degree in electrical engineering from Graz University of Technology, Austria, in 2000, and Ph.D. degree in electrical engineering from University of Leoben, Austria, in 2004. From 2005 to 2011 he worked as Postdoctoral Researcher, Research Associate and Senior Research Scientist at Edward L. Ginzton Laboratory, Stanford University, CA, USA. From 2011 to 2014, he was a full professor of electrical engineering at Brandenburg University of Technology, Cottbus, Germany. Since 2015, he has been a full professor at Technische Universität Darmstadt, Germany, where he is currently the head of the Measurement and Sensor Technology Group. His research topics are micromachined sensors and actuators, multiphysics simulations, flow metering of gases and liquids, ultrasound, electroacoustics, energy harvesting and harsh-environment instrumentation.